Al–SiO_2–Al Sandwich Microstrip Lines for High-Frequency On-Chip Interconnects

Jörg Gondermann, Elard G. Stein von Kamienski, Hartmut G. Roskos, and Heinrich Kurz

Abstract—**We present details on the high-frequency behavior of a downscaled 2 μm wide microstrip line, fabricated with both signal and ground conductors on top of the substrate. A significantly reduced geometric dispersion for electric pulses with a bandwidth of several hundred gigahertz is found in time-resolved electrooptic sampling measurements. Additionally, the strong confinement of the electric field within these surface-mounted microstrip lines promises low substrate losses, even on doped substrates, and reduced crosstalk.**

Introduction

MICROSTRIP transmission lines with a narrow signal conductor on the wafer surface and an extended ground plane on the backside are the most commonly used interconnects in millimeter-wave integrated circuits. Usually, the thickness of the semiconductor wafer defines the separation h of the signal conductor and the ground plane and is in the range from 100 to 500 μm. For frequencies of several gigahertz and above, this simple geometry limits its principally the useful bandwidth of ultrahigh-speed electronic circuits. Geometric dispersion distorts the electrical pulses propagating on the microstrip interconnects [1]. Furthermore, crosstalk and substrate losses become detrimental for the circuit performance.

The onset of geometric dispersion can be shifted to higher frequencies by reducing the separation h [2]–[6]. This is shown in Fig. 1 where the calculated effective dielectric constant of a microstrip is plotted as a function of frequency for different values of h. For a signal conductor width of 10 μm and a conductor separation of 2 μm, geometric dispersion remains negligible up to terahertz frequencies. An additional advantage of a reduced conductor separation is a better mode confinement with less capacitive coupling between neighboring lines.

Based on this principle, we have developed a downscaled 2 μm wide sandwich microstrip line sketched in Fig. 2. Both signal and ground conductors are placed on top of the wafer surface and separated by an 800 nm thick SiO_2 dielectric layer. A 500 nm thick bottom SiO_2 layer insulates the microstrip line from the semiconductor substrate. Such a waveguide configuration offers the following advantages: 1) The substrate losses are reduced because only a negligible part of the electromagnetic field leaks into the substrate. 2) The replacement of a semicon-

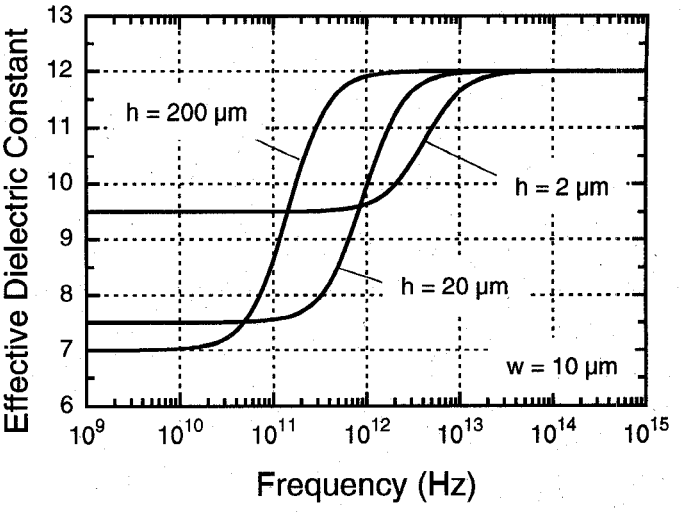

Fig. 1. Frequency dependence of the effective dielectric constant of a standard microstrip on silicon ($\epsilon_r = 12$) for different conductor separations h (center conductor width $w = 10$ μm). The onset of dispersion is shifted to higher frequency as the conductor spacing is narrowed [2]–[6].

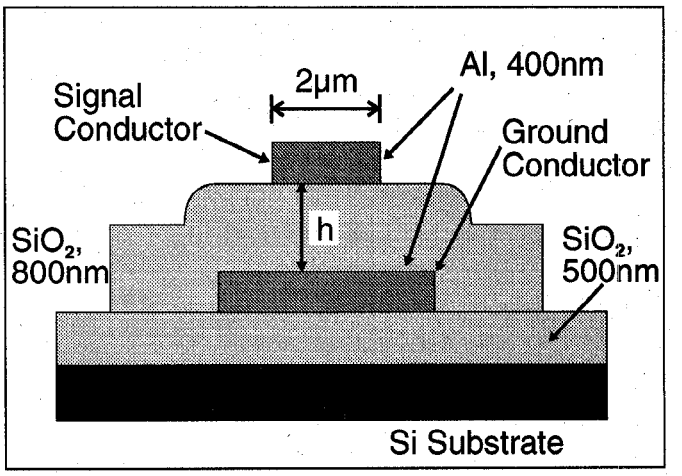

Fig. 2. Schematic of the cross section through the surface-mounted microstrip line. On the silicon substrate, an insulating SiO_2 layer is deposited, followed by the evaporation of an Al ground conductor. It is structured by optical lithography and wet etching. The structure is covered with another SiO_2 dielectric layer. On top of the dielectric, the Al signal conductor is manufactured using the same techniques.

Manuscript received March 29, 1993; revised June 18, 1993. This work was supported by the Ministry of Science and Technology of North-Rhine Westphalia.

The authors are with the Institut für Halbleitertechnik, RWTH (Rheinisch–Westfälische Technische Hochschule) Aachen, D-52056 Aachen, Germany.

IEEE Log Number 9212958.

ductor dielectric by SiO_2 reduces losses, too, because of the high resistivity of SiO_2 (about $10^{15}\ \Omega \cdot$ cm). 3) The propagation velocity of electrical signals is enhanced because of the low dielectric constant of SiO_2 ($\epsilon_r = 4$ compared to $\epsilon_r = 11$–13 of semiconductor substrates).

Device Fabrication

For the fabrication of our sandwich striplines, we use standard processes compatible to silicon VLSI fabrication technology (Fig. 2). A 500 nm thick insulating field oxide is deposited onto different silicon substrates by PECVD (plasma-enhanced chemical vapor deposition). For the determination of the influence of substrate qualities, we use both highly resistive silicon [(100), $>1000\ \Omega \cdot$ cm], and semiconducting silicon (p, (100), $5\ \Omega \cdot$ cm). Next, a 400 nm thick Al layer is deposited by *e*-beam evaporation. It is structured by optical lithography and subsequent wet etching for defining the ground conductor. A second 800 nm thick SiO_2 dielectric layer is deposited by PECVD and structured by RIE (reactive ion etching). The RIE process allows a good etch depth control and does not attack the Al ground conductor in the contact regions. On top of the dielectric, the 400 nm thick Al layer for the signal conductor is evaporated and again patterned by wet etching. In Fig. 3, a SEM cross section of the processed sandwich microstrip line is shown. The bright areas represent the Al conductors. The ground conductor is totally enclosed by SiO_2, while the signal conductor lies on top of the structure. On the left edge of the signal conductor, a fabrication-induced variation of the conductor's width is visible. Such width fluctuations may be responsible for undesirable multiple reflections which will be discussed below.

High-Frequency Characterization

For high-frequency characterization, the microstrip line is integrated into an impedance-matched coplanar line. As shown in Fig. 4, 100 μm long coupling regions are necessary to contact our vertical sandwich striplines with the coplanar lines used as terminals. In these coupling regions, the signal conductor experiences two steps: the first to the dielectric layer, and the second to the ground conductor. Unfortunately, these steps cause further reflection losses for the signals passing down the coupling segments.

The whole arrangement is connected by flip-chip technique to a coplanar photoconductive Auston switch [7] (see Fig. 5). It consists of a silicon-on-sapphire film between the conductors of a coplanar stripline. The carrier lifetime in the silicon is reduced by traps induced by radiation damage (Si-ion implantation, 350 keV, $5 \cdot 10^{14}/\text{cm}^2$). Ultrashort laser pulses (100 fs, colliding-pulse-mode-locked Rhodamine 6*G* laser) are focused on the biased Auston switch generating electrical pulses of 1.2 ps duration.

The propagation characteristics on the microstrip line are studied by electrooptic sampling based on the Pockels effect in an $LiTaO_3$ crystal [8], [9]. Due to the highly

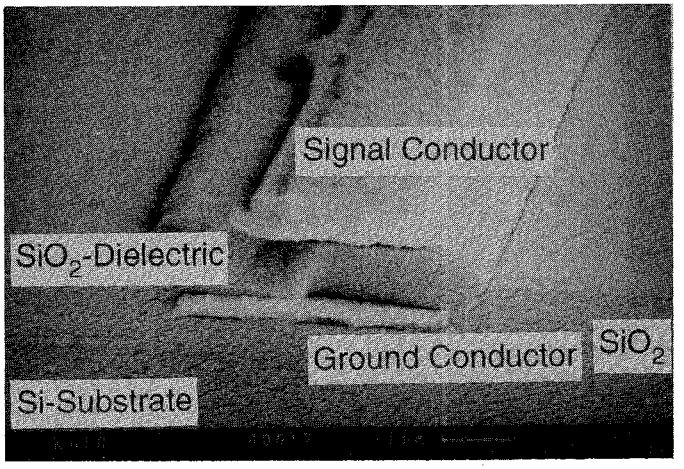

Fig. 3. SEM cross section of a sandwich microstrip line with both ground conductor and signal conductor on top of the substrate.

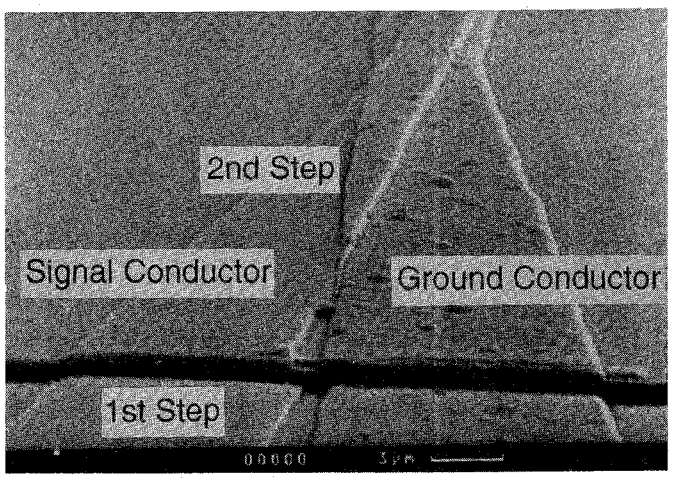

Fig. 4. SEM picture of the coupling section between coplanar stripline region used for contacting and the sandwich microstrip line itself. The signal conductor (left) on top of the microstrip line has to overcome two steps, causing reflection losses for electric signals.

confined field distribution, it is rather difficult to detect any electrical field on the stripline itself. Therefore, we measure the pulses in the coplanar regions in front of and after the microstrip line. The sampling points are indicated by arrows in Fig. 5. The electric field of the propagating pulse causes a variation of the polarization of the scanning laser pulse in the electrooptic crystal as illustrated in Fig. 6. This variation is detected and related to the electric field amplitude as a function of time.

Results and Discussion

Before presenting time-resolved data obtained with the sandwich microstrip, we briefly discuss the pulse propagation on a conventional microstrip line. Fig. 7 displays the detected waveform of an electrical pulse on such a line (width $w = 5\ \mu$m, $h = 500\ \mu$m) without coplanar couplers after propagation distances of 0.1, 1, and 2 mm (data taken from [6], supplemented by unpublished data). The ratio of the peak amplitudes of the original data for distances of 0.1 and 2 mm is 1 : 0.32. In this photoconductive sampling measurement, the bandwidth of the pulses was

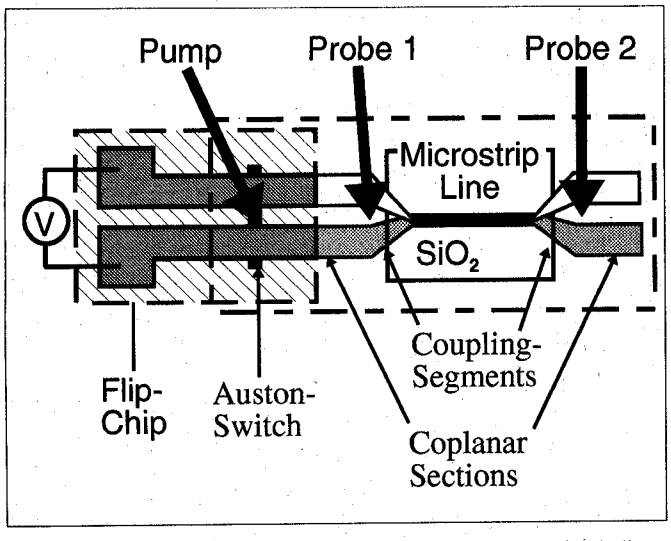

Fig. 5. Top view of the experimental arrangement. The arrows indicate the excitation spot on the flip-chip and the sampling spots in front of and behind the microstrip line.

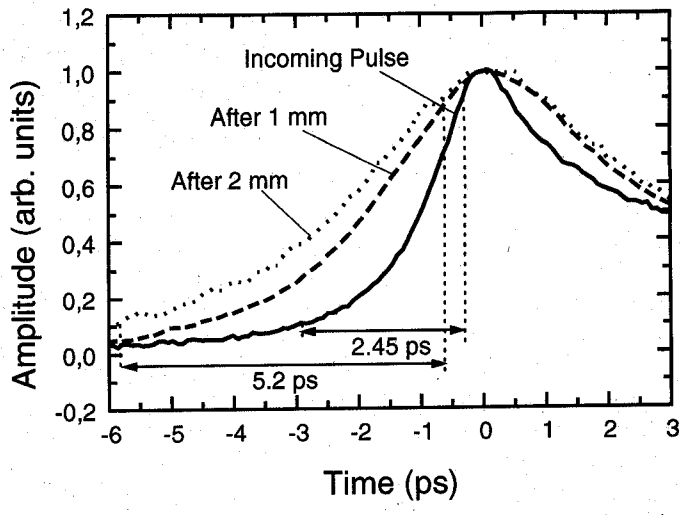

Fig. 7. Normalized detected electrical waveform on a standard microstrip line for the incoming pulse and after propagation distances of 1 and 2 mm. The time scale of each plot has been shifted so that the pulses are on top of each other. The ratio of the peak amplitudes of the original data for distances of 0.1 and 2 mm is 1 : 0.32.

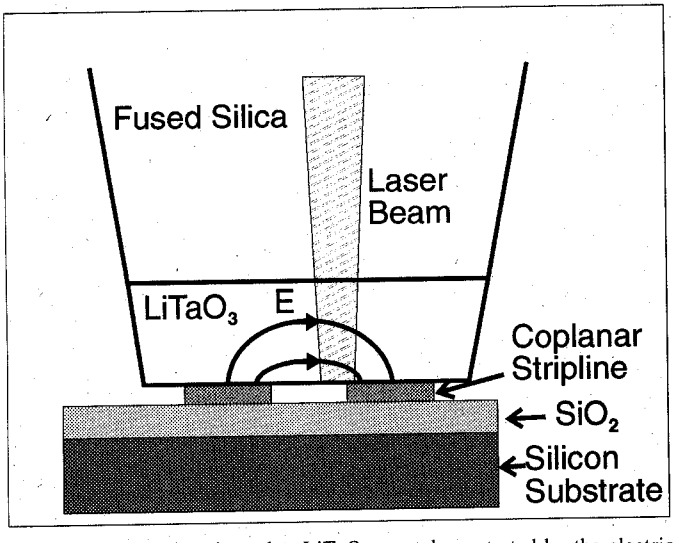

Fig. 6. Cross section through a $LiTaO_3$ crystal penetrated by the electric field of a signal propagating along a coplanar stripline.

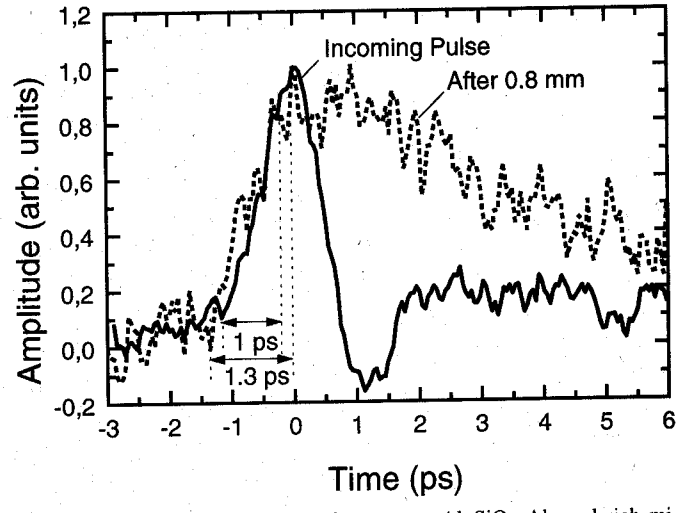

Fig. 8. Normalized detected waveform on an Al-SiO_2-Al sandwich microstrip line processed on a highly resistive silicon substrate. The signal conductor width is 2 μm. Waveforms are shown for the incoming pulse and after a propagation distance of 1 mm including the coplanar couplers. The amplitude ratio of the pulses is 1 : 0.19 (77 mV : 15 mV). The time scale of each plot has been shifted so that the pulses are on top of each other.

limited to 100 GHz. Dispersion manifests itself as an increase of the risetime (10–90%) from initially 2.45 to 5.2 ps after 2 mm propagation distance. Additionally, a ringing in the trailing part of the pulse occurs (not visible on the time scale of Fig. 7). Both result from the higher speed of the low-frequency components of the pulse.

In Fig. 8, we show for comparison normalized pulse propagation data of our sandwich microstrip lines on a highly resistive silicon substrate. The geometric dimensions of our microstrip line are $w = 2$ μm and $h = 800$ nm; the propagation distance on the microstrip line is 0.8 mm. In addition, a length of 0.2 mm for the coupling segments on each side has to be added. We use highly resistive material to avoid substrate losses in the coplanar coupling regions as well as in the microstrip line region. Although the material is highly resistive, the amplitude of the incoming pulse is only 77 mV, and the signals are fairly noisy. The amplitude ratio of these pulses is 1 : 0.19 (77 mV : 15 mV) and the bandwidth of the incoming pulse is about 400 GHz.

Despite the large bandwidth, the pulses show little geometric dispersion, with the rise-time increasing from 1 to 1.3 ps after 0.8 mm traveling. Comparing this rise-time with that of the conventional microstrip line, it is obvious that geometric dispersion of our microstrip line is drastically reduced. Also, a ringing in the trailing part of the pulse is not detected, but a pedestal emerges. This change of the pulseform may result from frequency-dependent losses. However, it is likely that multiple longitudinal reflections at the micro-rough metal surfaces (Fig. 3) contribute to this change of the waveform by redistributing

energy from the center of the pulse to its trailing part. To check this, the surface quality of the sandwich striplines has to be improved. Some data of another 0.8 mm microstrip line confirm this assumption: the signal conductor of this stripline has a width of $w = 1$ μm, so that the influence of width variations caused by surface roughness is more significant to the signal. In fact, the noise level increases in the trailing part of the outcoming pulse, but the rise-time remains fixed (1.1 ps). The absolute amplitudes are comparable with the data of Fig. 8 [the ratio of the pulses is 1 : 0.21 (69 mV : 15 mV)].

To examine the influence of the silicon substrate, we have produced sandwich microstrip lines on material with low resistivity (5 $\Omega \cdot$ cm). In Fig. 9, we show normalized pulse propagation data for these lines (again, $w = 2$ μm and $h = 800$ nm) for propagation distances of 0.8 and 1.6 mm plus coupling segments of 0.2 mm. The amplitude ratios are 1 : 0.35 : 0.25 (40 mV : 14 mV : 10 mV). Due to the losses in the coplanar coupling regions, the amplitude of the incoming pulse clearly decreases. Despite the large bandwidth of incoming pulses (again, 400 GHz), the rise-time increases only from 0.8 ps after 1 mm to 1.1 ps after traveling 1.8 mm. Therefore, geometric dispersion is negligible even for the long microstrip line on low-resistivity substrate. If we compare the pulses on low-resistivity silicon with the pulses on highly resistive silicon, no significant changes in pulseform are observed.

The losses on our microstrip line seem to be slightly higher compared to the standard microstrip line [6]. We attribute the decrease in pulse height from the incoming pulse to that detected after a distance of 0.8 mm (40–14 mV) mainly to leakage and reflections in the coplanar coupling segments in front of and at the end of the sandwich stripline. But the much smaller difference in peak amplitudes between the pulses measured after 0.8 and 1.6 mm (14–10 mV), respectively, is due to losses on the 0.8 mm long sandwich stripline alone (without the coupling regions). These losses are mainly caused by conductor losses because the total dimensions of our stripline are much smaller than in a standard microstrip line. In this case, we obtain an attenuation of 7.2 dB/mm from the ratios of the peak amplitudes (for the standard striplines 5.2 dB/mm). If we take other dispersion effects into account and compare the pulse energies instead of the peak amplitudes, an attenuation of 1.3 dB/mm is evaluated.

Based on these results, losses on our striplines seem to be independent of the substrate resistivity. This can be explained by a strongly confined field distribution for our sandwich microstrip line. This result indicates that our surface-mounted microstrip lines should be attractive for high-speed interconnects in highly integrated circuits, even when low resistive and active areas have to be crossed.

We have calculated the Fourier transforms analyzing the frequency spectra of the pulses on our microstrip line. As shown in Fig. 10, the bandwidth of the incoming pulse is in the range of 400 GHz. Below 100 GHz, the amplitude is reduced without significant frequency-dependence

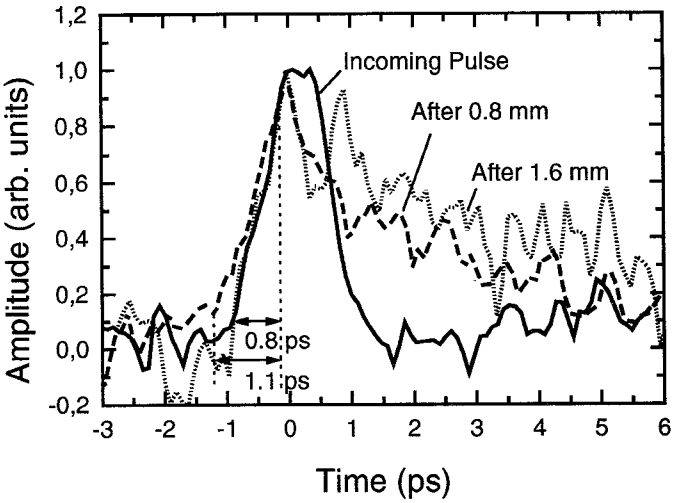

Fig. 9. Normalized detected waveform on an Al–SiO_2–Al sandwich microstrip line processed on a low-resistivity silicon substrate ($w = 2$ μm). Waveforms are shown for the incoming pulse and after propagation distances of 1 and 1.8 mm, including the coplanar couplers. The amplitude ratios of the pulses are 1 : 0.35 : 0.25 (40 mV : 14 mV : 10 mV). The time scale of each plot has been shifted so that the pulses are on top of each other.

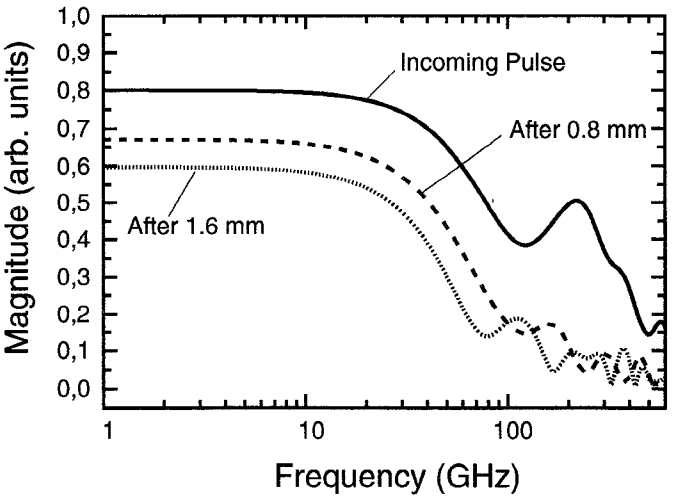

Fig. 10. Fourier transforms of the pulses on the sandwich microstrip line on low-resistivity substrate. Frequency spectra are shown for the incoming pulse and after propagation distances of 1 and 1.8 mm, including the coplanar coupler regions.

after passing the pulse through the microstrip line and the coupling segments. The frequency components above 100 GHz are more strongly damped.

In future experiments, the crosstalk behavior between neighboring and crossing sandwich striplines will be examined. Also, the quality of the metal surfaces has to be improved to reduce multiple reflections. One possibility may be an alternative dry etch technique in combination with thicker metallization.

Conclusions

In conclusion, we have developed a very compact microstrip line with both ground conductor and signal conductor on top of the wafer surface. The fabrication of our

downscale 2 μm Al-SiO_2-Al sandwich striplines is compatible to silicon VLSI technology. Due to the reduction of the total dimensions, the field distribution at this waveguides is highly confined, promising less crosstalk between densely packed interconnects. A further advantage of this confined field distribution is the negligible influence of the substrate resistivity upon the losses of our microstrip line. First examinations of propagation characteristics by time-resolved electrooptic sampling show low geometric dispersion for several-hundred-gigahertz bandwidth pulses.

ACKNOWLEDGMENTS

We acknowledge the help of Dr. Spangenberg in structuring the microstrip lines by RIE.

REFERENCES

[1] D. E. Cooper, "Picosecond optoelectronic measurement of microstrip dispersion," *Appl. Phys. Lett.*, vol. 47, pp. 33-35, July 1985.
[2] K. W. Gooseen and R. B. Hammond, "Modeling of picosecond pulse propagation in microstrip interconnections on integrated circuits," *IEEE Trans. Microwave Theory Tech.*, vol. 37, pp. 469-478, Mar. 1989.
[3] E. Hammerstad and Ø. Jensen, "Accurate models for microstrip computer-aided design," in *IEEE MTT-S Int. Microwave Symp. Dig.*, 1980, pp. 407-409.
[4] C.-Y. E. Tong and K. Wu, "Propagation characteristics of thin film superconducting microstrip line for terahertz applications," *Electron. Lett.*, vol. 27, pp. 2299-2300, Nov. 1991.
[5] R. L. Kautz, "Miniaturization of normal-state and superconducting striplines," *J. Res. Nat. Bur. Standards*, vol. 84, pp. 247-258, May-June 1979.
[6] H. Roskos, M. C. Nuss, K. W. Goosseen, D. W. Kisker, A. E. White, K. T. Short, D. C. Jacobson, and J. M. Poate, "Propagation of picosecond electrical pulses on a silicon-based microstrip line with buried cobalt silicide ground plane," *Appl. Phys. Lett.*, vol. 58, pp. 2604-2606, June 1991.
[7] P. R. Smith, D. H. Auston, A. M. Johnson, and W. M. Augustyniak, "Picosecond photoconductivity in radiation-damaged silicon-on-sapphire films," *Appl. Phys. Lett.*, vol. 38, pp. 47-50, 1981.
[8] J. A. Valdmanis, "Subpicosecond electrooptic sampling: Principles and applications," *IEEE J. Quantum Electron.*, vol. QE-22, pp. 69-78, Jan. 1986.
[9] M. Y. Frankel, J. F. Whitaker, and G. A. Mourou, "Optoelectronic transient characterization of ultrafast devices," *IEEE J. Quantum Electron.*, vol. QE-28, pp. 2313-2324, Oct. 1992.

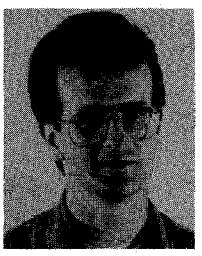

Jörg Gondermann was born in Bochum, Germany, on June 14, 1966. He received the diploma degree in electrical engineering from RWTH Aachen in 1992. His diploma thesis dealt with the fabrication and electrooptic characterization of high-speed waveguides.

He currently is a graduate student at the Institut für Halbleitertechnik II, RWTH Aachen, involved in the development of nanostructures in Si/SiGe using *e*-beam lithography.

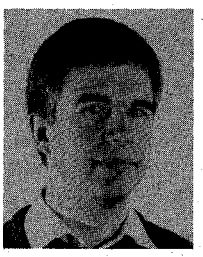

Elard G. Stein von Kamienski was born in Langenhagen, Germany, on February 23, 1965. He received the diploma degree in electrical engineering from RWTH Aachen in 1991.

Since 1991 he has been a graduate student at the Institut für Halbleitertechnik II, RWTH Aachen, working on the characterization of high-frequency circuits by electrooptic sampling. A second field of investigations are insulators on SiC.

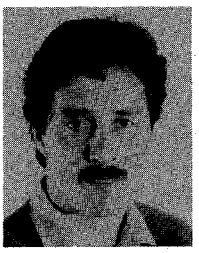

Hartmut G. Roskos studied physics at the Technical Universities of Karlsruhe and Munich, Germany. He received the diploma degree in 1985 and the Ph.D. degree in 1989, both from the Technical University of Munich.

From 1989 to 1991 he worked as a Postdoctoral Fellow at AT&T Bell Laboratories, Holmdel, NJ. In 1991, he joined the Institut für Halbleitertechnik II, RWTH Aachen, as a Research Assistant. He leads a group dealing with terahertz spectroscopy of semiconductor structures, high-speed device development, electrooptic high-frequency device characterization, nanostructure development, and novel materials for microelectronics such as high-T_c superconductors and SiC.

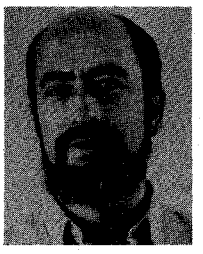

Heinrich Kurz was born in Pennewang, Austria. He received the Ph.D. degree in experimental physics from University Vienna, Austria, in 1971.

He joined the Philips Research Laboratories, Hamburg, Germany, from 1971 to 1981. From 1981 to 1984 he was with Harvard University, Cambridge, MA. He has been a Professor of Electrical Engineering since that time. His current research interests cover ultrafast solid-state phenomena, application of femtosecond laser technology, and high-speed device characterization. His Institute is also involved in research on Si-based nanostructures and novel materials for microelectronics such as SiC and high-T_c superconductors.